Version 2 TOMS UV algorithm: problems and enhancements

Nickolay Krotkov[1,2], Jay Herman[2], P.K.Bhartia[2], Colin Seftor[3], Antti Arola[4], Jussi Kaurola[4], Lasse Koskinen[4], S. Kalliskota [4], Petteri Taalas[4], I. Geogdzhaev[5]

[1] Goddard Earth Sciences and Technology Center, Univ. of Maryland Baltimore County;

[2]Laboratory for Atmospheres, NASA/Goddard Space Flight Center;

[3]Raytheon ITSS, Co.;

[4]Finnish Meteorological Institute;

[5]NASA/GISS and Columbia University.

[1]krotkov@chescat.gsfc.nasa.gov; phone 1 301 614 5553; Goddard Earth Sciences and Technology Center, Univ. of Maryland Baltimore County, NASA/Code 916, Greenbelt, MD, USA 20771;

ABSTRACT

Satellite instruments provide global maps of surface UV irradiance by combining backscattered radiance measurements with radiative transfer models. The models are limited by uncertainties in input parameters of the atmosphere and the surface. We evaluate the effects of possible enhancements of the current TOMS surface UV irradiance algorithm focusing on effects of diurnal variation of cloudiness and improved treatment of snow/ice. The emphasis is on comparison between the results of the current (version 1) TOMS UV algorithm and each of the changes proposed. We evaluate different approaches for improved treatment of pixel average cloud attenuation, with and without snow/ice on the ground. In addition to treating clouds based only on the measurements at the local time of the TOMS observations, the results from other satellites and weather assimilation models can be used to estimate attenuation of the incident UV irradiance throughout the day. A new method is proposed to obtain a more realistic treatment of snow covered terrain. The method is based on a statistical relation between UV reflectivity and snow depth. The new method reduced the bias between the TOMS UV estimations and ground-based UV measurements for snow periods. The improved (version 2) algorithm will be applied to re-process the existing TOMS UV data record (since 1978) and to the future satellite sensors (e.g., Quik/TOMS, GOME, OMI on EOS/Aura and Triana/EPIC).

Keywords: UV irradiance, TOMS, radiative transfer models, aerosols, clouds, snow albedo

1. INTRODUCTION

Global increases in UV-B fluxes from decreasing stratospheric ozone amounts[1-13] caused by anthropogenic chlorine releasing gases (mostly chlorofluorocarbons) have been an issue of public concern for the past 20 years because of their impact on human health, as well as terrestrial and aquatic ecosystems[14-20]. Several satellite-based methods for estimating UV irradiance have been suggested [4,8,21-37]. Because of long time record and global contiguous spatial coverage, the NASA Total Ozone Mapping Spectrometer (TOMS) data[38] were used for estimating global trends in surface UV irradiance[4, 8,24] and studying global UV climatology [28,31] (especially for regions not covered by ground-based UV networks and over oceans[39,40]). The TOMS UV record will continue with Ozone Monitoring Instrument[41] (OMI to be launched in 2004 on NASA EOS/Aura satellite) as the successor to TOMS.

First intercomparisons with ground-based UV measurements have indicated positive bias of the current (version 1) TOMS UV data for many locations in NH (~10% station-average overestimation under snow-free conditions [31,42-44,76]) and possible underestimation in the presence of snow [45]. Part of this bias can be attributed to the current (version 1) TOMS UV algorithm. The goal of this paper is to describe possible improvements to the operational TOMS UV algorithm[23, 27,31,36,41] that could help reducing this bias. Some of the proposed improvements will be implemented in the second version of the TOMS UV algorithm after extensive validation period (2002-2003). The improved (version 2) UV algorithm will be shared between TOMS and future GOME, TRIANA/EPIC and OMI UV products. The previous TOMS data record (since 1979) will be re-processed with the Version-2 UV algorithm to ensure homogeneity of the combined satellite global UV record for the trend analysis.

2. OVERVIEW OF THE CURRENT TOMS UV ALGORITHM

The amount of ultraviolet radiation in the UVA (320nm - 400nm) and UVB (290nm - 320nm) spectral ranges that reach the surface of the Earth is determined by Rayleigh scattering from the molecular atmosphere, the absorption of ozone, scattering by clouds, and both scattering and absorption by aerosols[5-13]. Current TOMS UV algorithm (version 1) is based on corrections to calculated clear-sky UV irradiance, E_{Clear} The calculation procedure is based on table lookup and either cloud/non-absorbing aerosol correction[36] or absorbing aerosol correction[27,31] (figure 1):

$$E_{cloud} = E_{clear} C_T \qquad (1)$$

Calculation of E_{clear} in the UV range from satellite-derived spectral extraterrestrial solar irradiance[46-49] and NASA's Total Ozone Mapping Spectrometer (TOMS) measurements of total column ozone, aerosols and surface reflectivity[38] was previously described in the literature[27,31], including estimates of the various error sources (Table 1). In the absence of snow, clouds, and aerosols, the effects of ozone, solar zenith angle, and altitude are essentially well-understood problems. However, presence of aerosols[50-55], clouds[5,10,13,21-36] and snow[56-58] in the satellite Field of View (FOV) requires additional corrections. The exact correction would require complete characterization of the optical state of the atmosphere and the surface during the course of the day (for daily exposure calculations). The complete information is never available from the satellite data alone. Therefore, the correction factor (C_T) has to be estimated using limited information available from the single satellite measurement at the overpass time. Currently, TOMS UV algorithm (version 1) estimates daily exposures assuming no diurnal changes in C_T factor ("frozen clouds and aerosols"). The type of correction (specific C_T

algorithm) is selected based on the two threshold values of the TOMS aerosol index (AI) (calculated from 340nm and 380nm radiances in case of Nimbus 7 TOMS and from 331nm and 360nm in case of Earth Probe TOMS) and Lambertian Equivalent Reflectivity (LER) (360nm or 380nm). The surface albedo and snow effects are estimated using the TOMS monthly Minimum Lambertian Effective surface Reflectivity (MLER) global databse[59,60] as described in [36,41].

3. IMPROVED CLOUD CORRECTION

The main cause of daily UV irradiance variability at a given geographic location is due to clouds. Polar orbiting satellites allow only one daily observation at a given location. Even at the overpass time both cloud fraction and cloud optical thickness cannot be simultaneously derived on the basis of one TOMS radiance measurement. Currently, to estimate the cloud transmittance at the overpass time TOMS algorithm uses homogeneous cloud model embedded into Rayleigh scattering atmosphere with known ozone absorption and surface reflectivity, A_S, assuming 100% cloud cover [36,41]. For snow-free conditions in the near UV spectral region A_S is uniformly low and can be accurately predicted from a climatological data base that was developed using 15 years of TOMS data[59]. The "effective" cloud optical thickness, $\tau(t_0)$, is derived by matching the measured 380nm radiance at the overpass time, t_0, with the calculated radiance for each TOMS FOV. The same cloud model is used to calculate the $C_T(t_0)$ as a function of $\tau(t_0)$, A_S, and solar zenith angle,θ_0, at all UV wavelengths, assuming spectrally independent $\tau(t_0)$:

$$C_T(\lambda, t_0) = C_T(\lambda, \tau(t_0), A_S, \theta_0(t_0)) \qquad (2)$$

The method accounts for the spectral dependence of C_T (resulted from reflection between the cloud and the atmosphere) as well as multiple reflections between the cloud and the surface. The second effect is especially important for snow covered surfaces. To calculate daily exposure, diurnal variation of $C_T(\lambda,t)$ should be estimated. For TOMS, only one observation per day is available for low- and midlatitude locations. Therefore, the TOMS algorithm assumes that cloud transmittance is the same as at overpass time:

$$C_T(\lambda,t) = C_T(\lambda,t_0) \qquad (3)$$

This may lead to erroneous UV-exposure estimates for areas with systematic changes in cloudiness during the day. An obvious example of such a case is for cumulus clouds, which commonly develop during afternoon hours (Figure 2).

3.1 Assimilating ECMWF water content to construct a time-resolved homogeneous cloud model

To improve daily exposure estimates additional cloudiness information per day is needed. Such information is available from global operational weather models and from geostationary satellites (GOES, Meteosat) [32]. For example, one can use vertically integrated cloud parameters (total cloud cover, T_C, total column water and ice content, LWC(t) provided by numerical model of the European Center for Medium Range Weather forecasts (ECMWF). Global ground-based, balloon borne and satellite weather observations are used for producing global 3-dimensional analysis every 3 hours (http://www.ecmwf.int/). The spatial resolution of the Center's current model is equivalent to having

gridpoints separated by ~60 km around the globe. The estimated daily data volume is ~20-30MB/day. The easiest way of assimilating the model parameters into the TOMS UV processing algorithm is to scale TOMS effective cloud optical depth proportionally to the diurnal changes of the ECMWF model total column water and ice content, LWC(t):

$$C_T(\lambda,t) = C_T(\lambda, \tau(t\ ), A_S, \theta_0(t\ )) \qquad (4)$$

$$\tau(t) = \tau_0(t_0)\frac{\tau_E(t)}{\tau_E(t_0)}$$

where τ_E is ECMWF cloud optical depth, estimated from the total column water and ice content, assuming homogeneous cloud layer with C1 droplet size distribution. The algorithm becomes computationally unstable when $LWC(t_0)$ (and $\tau_E(t_0)$) approaches zero or there are large disagreements between the model and TOMS estimates of the cloud optical thickness at the overpass time. In such cases, the following algorithm could be suggested that is computationally stable:

$$\tau(t) = \tau(t_0) + \tau_E(t) - \tau_E(t_0)$$

We note that above equation reduces to equation (4) if the TOMS and model optical thickness agree at the overpass time: $\tau(t_0) = \tau_E(t_0)$. The scheme also works when either $\tau(t_0)=0$ *or* $\tau_E(t_0)=0$. If TOMS and ECMWF values are far apart at the overpass time (which is not uncommon), the above equation gives more reasonable values of optical thickness than equation (4).

An example of the methodology is shown in Figure 2, which shows the daily evolution of LWC(t) and UV radiation as measured by Brewer instrument on 10 August 1992 at Sodankylä (Finland). According to the model (and SYNOP observations) both T_C and LWC(t) increased during that day. The UV dose rates calculated with the old (Equation 3) and new (Equation 4) versions of TOMS UV algorithm are shown with approximately 10-minute time step. The dose rates calculated by the original algorithm (closed circles - equation 3) follow closely the clear-sky dose rates (open circles) because the overpass time (t_0= 8UTC) was almost cloud-free. As a result, the original method overestimates the daily UV dose by 60% as compared with the ground-based data while the new algorithm (Equation 4) is close to the observation.

The proposed daily-exposure cloud algorithm was tested using combined noontime TOMS and 3-hour ECMWF data for summer 1992 at Sodankylä (Figure 3). The overall performance of the new algorithm is better than the old one: the mean difference between the TOMS UV and Brewer data reduced from 182 J/m^2 to 126J/m^2 during the period, at the same time correlation increased from 0.86 to 0.89. The improvement is better than the absolute numbers indicate, since a substantial portion (about half) of the current bias between the TOMS and the Brewer measurements is not related to the TOMS cloud algorithm[31].

These results present a first-guess implementation using only water content time-resolved cloud data from the ECMWF model. Fine-tuning of the cloud algorithm will be performed to improve the agreement between the observed and the improved cases further. In the TOMS UV project the global comparability between different cloud models will be studied (i.e. ECMWF, NOAA-NCEP, NASA-

Goddard, NASA-ISCCP models), and improvements in the methodology will be made if needed. For example, we plan to compare cloud data from the ECMWF model with the similar data from International Satellite Cloud Climatology Project (ISCCP -http://isccp.giss.nasa.gov/) when both are available. ISCCP analysis combines satellite-measured radiances from geostationary and polar satellites with ice/snow data to obtain information about clouds and the surface[61]. The pixel analysis is performed separately for each satellite radiance data set and the merged results are reported in the Stage DX data product, which has a nominal resolution of 30km and 3 hours. Using ISCCP data operationally for TOMS processing is currently impossible due to the large time delay in releasing ISCCP data products. The ISCCP data may be used for future re-processing of the global TOMS UV maps. We will also analyze possibility of using single satellite time-resolved cloud information in producing regional UV maps and overpass data sets. One possibility may be using Meteosat Second Generation (MSG) Climate SAF products for producing European UV maps[32] and NOAA-GOES data for US coverage.

3.2 Assimilating ECMWF cloud fraction and water content with a fractional cloud model

The overestimation of the TOMS UV data for high irradiance levels (Figure 3) may be related to the broken cloud effects. The ECMWF model can be combined with a fractional cloud model[62] since it contains the cloud cover information, $T_c(t)$. We will study a possibility to use both T_C and water content from the ECMWF model to improve estimation of C_T. First, the ECMWF cloud parameters should be adjusted using TOMS radiance measurement at the overpass time. For areas where there are

ground-based measurements or a region with specific biological interest, the cloud pattern data from high resolution satellite images (ATSR-2, AVHRR, SeaWiFs, geostationary satellites e.g., GOES) can be also used to estimate true cloud fraction, $T_C(t_0)$, so the ECMWF model data can be adjusted. Second, the effective optical depth of the cloud portion of the TOMS FOV, $\tau_F(t_0)$ can be derived by matching the TOMS measured and pre-calculated radiances at the overpass time:

$$I^{Measured}(t_0) = T_c(t_0) I^{Calc}_{cloud}(\tau_F(t_0)) + (1 - T_C(t_0)) I^{Calc}_{Clear} \qquad (5)$$

Finally, the ECMWF time resolved cloud data, normalized by the $T_c(t_0)$ and $\tau_F(t_0)$, can be used to predict diurnal variation of $C_T(t)$, similar to equation (4):

$$C_T(t) = 1 - T_C(t)[1 - C_T(\lambda, \tau_F(t), R_S, \theta_0)] \qquad (6)$$

3.3 Cloud shape effects

The fractional cloud model described ignores the real 3-dimensional (3D) cloud structure and some related cloud-radiation effects (cloud shadows, reflection from non-horizontal surfaces). We will estimate "cloud shape" errors and develop average C_T corrections for the TOMS FOVs using more realistic cloud models and Monte-Carlo radiative transfer code[63]. Figure 4 shows one possible cloud model, which describes fair weather cumulus cloud field. The model relates stochastic field characteristics with cloud amount, mean cloud diameter and aspect ratio. Based on these input

parameters a representation of cloud field is calculated as convolution of two-dimensional Fourier series with random coefficients. Calculations of the radiance at the top of the atmosphere and irradiance at the surface are performed using 3-D Monte-Carlo (MC) code[63].

Figure 5 shows the simulated normalized angular distribution of the 380nm radiance (Anisotropic function, AIF[64]) backscattered from the cloud scene shown in Figure 4. The "cloud shape" error in surface irradiance is proportional to the AIF ratio for broken (Figure 5) and homogeneous cloud scenes averaged over TOMS FOV. The error is a function of assumed cloud parameters, observational geometry, and surface albedo. Figure 6 shows the correction factor for cloud scene shown in figure 4. The factor should be applied to the standard C_T value calculated using the optically equivalent (i.e. providing the same 380nm radiance at the satellite) homogeneous cloud model (see Equation 2). As expected, the factor is maximal in the solar principal plane. For this particular cloud scene and $\theta_o=54^o$ the factor ranges from 0.85 ($\varphi=0^o$- forward reflecting) to 1.2 ($\varphi=180^o$ – backward reflecting, i.e. "hot spot").

Because the equatorial overpass occurs close to solar noontime, the TOMS instrument scans in a direction, which is approximately perpendicular to the principal plane of the sun. Figure 6 shows that for these directions the correction factor is much less than in the solar principal plane. However, the errors may be still significant for specific observational conditions (we found that the error increases with solar zenith angle, i.e. at high latitudes). To quantify the errors for all possible conditions the 3D Monte-Carlo broken cloud radiative transfer model will be combined with realistic snow BRDF (Bidirectional Reflection Distribution Function) to calculate the surface UV irradiance over snow with broken cloud conditions. Preliminary calculations have shown that broken cloud effects over snow differ from the uniform cloud effects over snow surface. The broken cloud model will be also

combined with tropospheric aerosol models to study combined cloud/ aerosol / radiation interactions. Before adopting either of these approaches in the version 2 TOMS UV algorithm we perform validation studies using radiative transfer modeling and comparisons with ground-based UV data for selected stations.

4. SNOW EFFECTS

A major problem in using satellite data to estimate UV irradiance at high latitudes arises from the difficulty in identifying the presence of clouds when there is snow on the ground. When TOMS views a scene containing ice, snow, and clouds there is no way to separate the effects of snow from clouds based on one reflectivity measurement. However, if the surface reflectivity (albedo), A_S is established for various conditions in a geographical region, the excess scene reflectivity can be used to estimate cloud transmittance, C_T, over snow surface[36,41]. Current TOMS UV algorithm uses monthly minimal Lambert equivalent surface reflectivity (MLER) global database[59,60] to estimate A_s at 380nm. The algorithm also assumes that A_S does not change with wavelength in the UVA and UVB spectral regions. The assumption are in reasonable agreement with direct ground-based measurements of UV albedo[5,7,56-58,65-66]. MLER is a reasonable estimate of the surface albedo for either snow-free conditions or regions with permanent snow cover (Antarctica, Greenland). However, MLER is not a good estimator of actual surface albedo at mid-latitudes in spring and fall seasons when surface albedo varies daily depending on the presence and state of snow cover. In absence of external snow information the current TOMS algorithm uses a climatological snow/ice flag (probability of the presence of snow on a given day at a given location) to detect the presence of snow. If snow is detected (or likely), the algorithm first determines a snow albedo threshold (SAT). Currently the SAT is the

MLER value bounded by a constant value of 0.4. The value 0.4 was selected as appropriate for snow covered urban/suburban-populated areas containing at least moderate densities of roads, houses, and trees (e.g., Toronto, Moscow)[36,41]. The daily estimation of A_S is based on comparison of SAT with the TOMS measured reflectivity (LER) at 380nm (or 360nm). If LER is less than SAT+0.05, the cloud free conditions are assumed and A_S is set equal to LER (C_T=1). If LER is more than SAT+0.05, A_S is set equal to SAT and all additional measured reflectivity is assigned to a cloud above the snow surface. The algorithm proceeds to calculation of effective cloud optical thickness and C_T as described above. The constant threshold value 0.05 was chosen because of the difficulty in detecting thin clouds over snow surface. This problem exacerbates at high latitudes over areas with permanent snow cover (Greenland, Antarctica). For such regions, the possible error in cloud correction could exceed the error due to neglecting the clouds. Therefore, cloud free conditions are also assumed if the SAT value is more than 0.9. On average, current TOMS algorithm leads to underestimation of UV radiation in winter conditions [35,37,45].

To obtain a more realistic treatment of the albedo of snow covered terrain, a new method was developed[67]. This method is based on a relation between UV reflectivity and snow depth. To establish such a relationship cloudless days with snow cover were selected based on the total cloud cover and snow depth (SD) parameters of the ECMWF ERA-15 re-analysis dataset (covering time period 1979-1994). These data together with the coincident and co-located Nimbus-7 TOMS reflectivity measurements were used to set a regression:

$$\text{Albedo} = a \times SD^{1/3} \qquad (7)$$

where a is fit parameter specific to each ground pixel. As expected, this method improved the correspondence between the satellite-retrieved results and ground-based measurements (figure 7).

5. AEROSOL EFFECTS

For the purposes of estimating UV irradiance at the Earth's surface, there are two classes of aerosols that must be considered: 1) aerosols that only scatter UV radiation and 2) aerosols that both scatter and absorb UV radiation. The first category is included in the measured scene reflectivity (cloud optical thickness) and attenuates UV radiation in a manner that approximates clouds of equivalent reflectivity, except for the spectral dependence of the optical thickness and phase function differences. Attenuation values of up to 10% are common. Operational (Version 1) TOMS UV algorithm does not distinguish between water clouds, haze, ice clouds and non-absorbing aerosols. This could result in a few percent errors when a non-absorbing aerosol layer is treated as an optically thin cloud of the same reflectance. The error due to non-absorbing aerosols could be both positive and negative depending on the observational geometry (phase function effect) and could be treated as a random error, rather than the constant bias.

On the other hand, a significantly larger overestimation occurs if absorbing aerosol is treated as non-absorbing or clouds[27]. Radiative transfer calculations with different absorbing aerosols models (industrial, smoke, dust) have shown a positive bias of the TOMS UV data if absorbing aerosols are treated as non-absorbing clouds. The bias is always positive (TOMS overestimates surface UV irradiance) and is proportional to the aerosol absorption optical thickness, which is a product of

extinction optical thickness and single scattering co-albedo (ratio of aerosol column absorption to the sum of absorption and scattering). The properties of absorbing aerosols vary depending on location, season, pollution and aerosol transport. Therefore, to characterize the bias for particular region a joint statistics of aerosol optical thickness and UV single scattering albedo is required. Not until recently such joint statistics becomes available from the inversions of the AERONET sun and sky photometer measurements[70-75]. The AERONET retrievals of single scattering albedo are currently restricted to the visible spectral region (shortest wavelength 440nm) and the retrieval uncertainties are large for a relatively clean locations (aerosol optical thickness less than 0.5) covering most of the globe. Therefore, the problem of extrapolating AERONET data from the visible to the UV spectral region remains a big challenge.

Under certain favorable conditions absorbing aerosol plumes transported in a free troposphere (dust and biomass burning smoke plumes at high altitudes) can be detected directly using the TOMS Aerosol Index (AI) data[68,69]. For such cases (mostly in tropical regions) the cloud correction is replaced by absorbing aerosol correction (AAC) algorithm [27,31]. The AAC algorithm accounts for larger attenuation of UV irradiance by absorbing aerosols compare to clouds/non-absorbing aerosols of the same reflectivity (see figure 1). Currently, the AI data are used directly to correct E_{lear} (1) for attenuation by absorbing aerosols:

$$\frac{E_{aerosol}}{E_{Clear}} = e^{-g(H_A)AI} \qquad (8)$$

where conversion factor g is a function of aerosol height, H_A and aerosol type. For the AAC method the major problem arises from uncertainty in aerosol plume height. Current TOMS AAC algorithm assumes the nominal height of 3km for plumes of desert dust and biomass burning smoke in the tropics [27,31]. The uncertainty in the actual aerosol height is included in the error budget of the TOMS UV products as shown in table 2[31]. In the second version of the TOMS UV algorithm the H_A could be estimated using the GSFC data assimilation model or other sources.

The AAC technique does not have the sensitivity to detect weakly absorbing aerosols in the boundary layer. This is the main reason of overestimating surface UV under cloud-free conditions for industrial regions. The treatment of aerosol attenuation of UV irradiance might have been improved by using newly developed TOMS aerosol products: optical depth and single-scattering albedo for dust, smoke, and sulfate aerosols[69]. However, the method requires a-priori knowledge of the aerosol vertical distribution and information about aerosol parameters (either size distribution or refractive index). Complete aerosol retrieval is possible by combining TOMS measurements with ground-based active (lidar) or passive (sun and sky photometer) measurements. Combining the TOMS data with sun-photometer (AERONET network) and lidar data appears to be the most perspective way of improving aerosol correction algorithm for regions affected by smoke from biomass burning or desert dust. However, characterization of the aerosol properties (size distribution and single-scattering albedo) in an atmospheric column from the sky photometer measurements becomes increasingly challenging for small amounts of absorbing aerosols. In addition, presence of broken clouds adds to the uncertainty of both ground-based and TOMS aerosol retrievals. Thus, improving characterization of the average transmittance through the inhomogeneous scenes including mixtures of broken clouds with absorbing aerosols remains the most challenging problem in satellite UV estimation.

6. CONCLUSIONS

We evaluated the effects of possible enhancements of the current (version 1) TOMS surface UV irradiance algorithm. The enhancements include more detailed treatment of tropospheric aerosols, effects of diurnal variation of cloudiness and improved treatment of snow/ice. Some of the proposed improvements will be implemented in the second version of the TOMS UV algorithm after extensive validation period (2002-2003). Validation of spatial average UV irradiance (satellite) with temporal average UV data (ground station) under broken cloud conditions would require implementation of special sub-satellite UV validation campaigns and optimal ground UV validation strategy.

ACKNOWLEDGEMENTS

The work was supported by the NASA TOMS project.

REFERENCES

1. R.S. Stolarski, P.Bloomfield, R.D. McPeters, and J.R. Herman, Total ozone trends deduced from Nimbus 7 TOMS data, Geophys. Res. Lett., 18, 1015-1018 (1991)

2. Herman, J.R., and D. Larko, "Low ozone amounts during 1992 and 1993 from Nimbus 7 and Meteor 3 total ozone mapping spectrometers", J. Geophys.Res., 99, 3483-3496 (1994)

3. McPeters, R. D., S. M. Hollandsworth, L. E. Flynn, J. R. Herman, and C. J. Seftor, Long-term ozone trends derived from the 16-year combined Nimbus 7/Meteor 3 TOMS Version 7 record, Geophys. Res. Lett., 23, 3699-3702 (1996).

4. S. Madronich, "Implications of recent total ozone measurements for biologically active ultraviolet radiation reaching the Earth's surface", Geophys. Res. Lett., 19, 37-40 (1992).

5. S. Madronich, "The atmosphere and UV-B Radiation at ground level", In Environmental UV Photobiology, edited by A. R.Young et al., Plenum Press, New York, pp.1-39 (1993).

6. A.F. Bais, C.S.Zerefos, C.Meleti, I.C.Ziomas, and K. Tourpali, "Spectral measurements of solar UVB radiation and its relations to total ozone, SO_2, and clouds", J. Geophys. Res., 98, 5199-5204 (1993)

7. R.L. McKenzie, M.Kotkamp, and W.Ireland, "Upwelling UV Spectral irradiances and surface albedo measurements at Lauder", New Zealand, Geophys. Res. Lett., 23, 1757-1760 (1996).

8. J.R. Herman, P.K.Bhartia, Z. Ahmad, and D.Larko, "UV-B radiation increases (1979-1992) from decreases in total ozone," Geophys. Res. Lett., 23, pp. 2117 – 2120 (1996).

9. V.E. Fioletov, J. B. Kerr, D. I. Wardle, The relationship between total ozone and spectral UV irradiance from Brewer observations and its use for derivation of total ozone from UV measurements, Geophys. Res. Lett., 24 , 2997-3000 (1997).

10. V.E. Fioletov and W.F.J. Evans, The influence of ozone and other factors on surface radiation, In: Ozone Science: a Canadian Perspective on the changing ozone layer, Edited by D.I.Wardle, J.B.Kerr, C.T. McElroy, and D.R. Francis, CARD 97-3, Environment Canada Report, pp. 73-90 (1997).

11. N.B. Chubarova, Ultraviolet radiation under broken cloud conditions as inferred from many-year ground-based observations, Izvestiya, Atmospheric and Oceanic Physics, 34, 131-135 (1998).

12. Sabziparvar, A.A., P.M. de F. Forster, and K.P.Shine, Changes in ultraviolet radiation due to stratospheric and tropospheric ozone changes since preindustrial times, *J. Geophys. Res.*, 103, 26107-26113, (1998).

13. WMO98, Herman,J.R., R. L.McKenzie, S.B.Diaz, J.B.Kerr, S.Madronich, and G.Seckmeyer, "Ultraviolet radiation at the Earth's surface", Chapter 9 In: Scientific Assesment of Ozone Depletion: 1998, World Meteorological Organization, Global Ozone Research and Monitoring Project – Report N0.44, ISBN:92-807-1722-7, Geneva, Switzeland, (1999).

14. International Arctic Science Committee (IASC), "Effects of Increased Ultraviolet Radiation in the Arctic, An interdisciplinary report on the state of knowledge and research need", IASC Report N2, available from IASC Secretariat , Middelthus Gate 29, P.O.Box 5072, Majorstua, 0301 Oslo, Norway, (1996).

15. D.L. Leffell and D.E. Brash, 1996, "Sunlight and Skin Cancer", Scientific American, 52-59 (1996).

16. SCOPE, "Effects of increased ultraviolet radiation on biological systems. Scientific Commitee on Problems of the Environment (SCOPE)", 51 bd de Montmorency, 75016 Paris, France (1992).

17. SCOPE, Effects of increased ultraviolet radiation on global ecosystems. Scientific Commitee on Problems of the Environment (SCOPE), 51 bd de Montmorency, 75016 Paris, France, 1993

18. R.C. Smith, B.B.Prezelin, K.S. Baker, R.R.Biligare, N.P.Boucher, T.Coley, D.Karentz, S.MacIntyre, H.A.Matlic, D.Menzies, M.Ondrusek, Z.Wan, K.J.Waters, "Ozone depletion: ultraviolet radiation and phytoplankton biology in Antarctic waters", Science, 255, 952-959 (1992).

19. C.S Weiler., and P. A. Penhale, Eds. "Ultraviolet Radiation in Antarctica: Measurements and biological Effects", AGU, Antarctic Research series, 62, 257 (1994).

20. United Nations Environmen Programme (UNEP) "Environmental Effects of Stratospheric Ozone Depletion - 1994 Assessment" eds J.C. van der Leun, A. H.Teramura, and M.Tevini) UNEP, Nairobi, Kenya (1994).

21. J.E. Frederick and D. Lubin, The budget of Biologically active ultraviolet radiation in the Earth-Atmosphere system, *J. Geophys. Res.*,93(D4), 3825-3832 (1988).

22. D. Lubin, P.Ricchiazzi, C.Gautier, and R.H.Whritner, "A Method for Mapping Antarctic surface ultraviolet radiation using multispectral satellite imagery", In: Ultraviolet Radiation in Antarctica: measurements and biological effects, Weiler, C.S., and P. A. Penhale, Eds., AGU, Antarctic Research series, 62, 53-82 (1994).

23. T.F. Eck, P.K.Bhartia, and J.B. Kerr, Satellite Estimation of spectral UVB irradiance using TOMS derived ozone and reflectivity, *Geophys. Res. Lett.*, 22, 611-614 (1995).

24. D. Lubin, D. and E.H.Jensen, "Effects of clouds and stratospheric ozone depletion on ultraviolet radiation trends", *Nature*, 377, 710-713 (1995).

25. C.S. Long, A.J.Miller, H.T.Lee, J.D.Wild, R.C.Przywarty, and D. Hufford, "Ultraviolet Index forecasts issued by the National Weather Service", *Bull. Amer. Meteorol. Soc.*, 77, 729-747 (1996).

26. R. Meerkoetter, B.Wissinger, and G.Seckmeyer, Surface UV from ERS-2/GOME and NOAA/AVHRR data: A case study, *Geophys. Res. Lett.*, 24, 1939-1942 (1997).

27. N.A. Krotkov, P.K.Bhartia, J.R.Herman, V.Fioletov, J.Kerr, "Satellite estimation of spectral surface UV irradiance in the presence of tropospheric aerosols 1. Cloud-free case," *J. Geophys. Res.*, 103, pp. 8779-8793 (1998).

28. D. Lubin, E.H.Jensen, and H.P. Gies, "Global surface ultraviolet radiation climatology from TOMS and ERBE data", *J.Geophys. Res*, 103, 26061-26091 (1998).

29. B. Mayer, C.A. Fischer, and S.Madronich, "Estimation of surface actinic flux from satellite (TOMS) ozone and cloud reflectivity measurements", *Geophys. Res. Lett.*, 25, 4321-4324 (1998).

30. P. Peeters, J.F. Muller, P.C. Simon, E. Celarier, and J.R. Herman, Estimation of UV flux at the Earth's surface from GOME data, ESA, *Earth Observation*, 58, 39-40 (1998).

31. J.R.Herman, N.Krotkov, E.Celarier, D.Larko, and G.Labow, "The distribution of UV radiation at the Earth's surface from TOMS measured UV-backscattered radiances," *J. Geophys. Res.*, 104, 12059-12076 (1999).

32. J. Verdebout, "A method to generate surface UV radiation maps over Europe using GOME, Meteosat, and ancillary geophysical data", *J. Geophys. Res.*, 105, 5049-5058 (2000).

33. J. Matthijsen, H.Slaper, and H.A.J.M.Reinen,G.J.M. Velders, "Reduction of solar UV by clouds: Comparison between satellite-derived cloud effects and ground-based radiation measurements", *J.Geophys.Res.*,105, 5069-5080 (2000).

34. Z. Li, P.Wang, and J. Cihlar, "A simple and efficient method for retrieving surface UV radiation dose rate from satellite", *J. Geophys. Res.*, 105, 5027-5036 (2000).

35. S. Kalliskota "Some approaches to estimate UV radiation reaching the Earth's surface by using satellite data and their validation", Licentiate dissertation, Univ. of Helsinki, (2001).

36. N.A. Krotkov, J.R.Herman, P.K.Bhartia V.Fioletov and Z.Ahmad, "Satellite estimation of spectral surface UV irradiance 2. Effects of homogeneous clouds and snow," *J. Geophys. Res.* 106, (2001).

37. A. Arola, S. Kalliskota, P.N den Outer, K. Edvardsen, G. Hansen, T. Koskela, T. J. Martin, J. Matthijsen, R. Meerkoetter, P. Peeters, G. Seckmeyer, P. Simon, H. Slaper, P. Taalas and J. Verdebout, Four UV mapping procedures using satellite data and their validation against ground-based UV measurements, *J. Geophys. Res*, 107, accepted, 2002

38. McPeters, R.D., P.K.Bhartia, A.J.Krueger, J.R.Herman, B.M.Schlesinger, C.G.Wellemeyer, C.J. Seftor, G.Jaross, S.L.Taylor,T.Swissler, O.Torres, G.Labow, W. Byerly, and R.P.Cebula, Total ozone Mapping Spectrometer (TOMS) Data Products User's Guide, NASA Ref.Publ. No 1384, 1996

39. A.P. Vasilkov, N. Krotkov, J.R. Herman, C. McClain, K. Arrigo, and W. Robinson, "Global mapping of underwater UV irradiance and DNA-weighted exposures using TOMS and SeaWiFS data products," *J. Geophys. Res*, 106, 27205-27219 (2001).

40. A.P. Vasilkov, J.R. Herman, N. Krotkov, Greg Mitchell, and Mati Kahru, "Problems of assessment of UV penetration into natural waters from space based measurements," SPIE proceedings (2001).

41. N.A.Krotkov, J.R. Herman, P.K.Bhartia, C. Seftor, A. Arola, J. Kaurola, L. Koskinen, P. Taalas, S.Kalliskota, and T. Tikkanen, "OMI surface UV irradiance algorithm" In: Ozone Monitoring Instrument (OMI) Algorithm Theoretical Basis Document, volume 3 "Aerosol, Clouds and surface UV irradiance", ed. P.Stammes , KNMI (2001).

42. N.Chubarova, Alla Yu. Yurova , Nickolay A. Krotkov , Jay R. Herman , PK. Bhartia, "Comparisons between ground measurements of UV irradiance 290 to 380nm and TOMS UV estimates over Moscow for 1979-2000", SPIE Proceedings (2001).

43. J.Slusser, J.R.Herman, W.Gao, N.A.Krotkov,G.Labow, G.Scott, "Comparison of USDA UV shadowband irradiance measurements with TOM Ssatellite retrievals and DISORT model under all sky conditions, SPIE Proceedings, Ed. Jim Slusser (2001).

44. V.E.Fioletov J.B.Kerr, D.I.W#ardle, N.A.Krotkov,J.R.Herman, "Comparison of Brewer UV irradiance measurements with TOMS satellite retrievals", Proceedings SPIE (2001).

45. S.Kalliskota, J.Kaurola, P.Taalas, J.R.Herman, E.A.Celarier, and N.Krotkov, "Comparison of daily UV doses estimated from Nimbus 7/TOMS measurements and ground-based spectroradiometric data", *J.Geophys.Res.*,105, 5059-5067 (2000).

46. G.E. Brueckner, et al., "The Solar Ultraviolet Spectral Irradiance Monitor (SUSIM) on board the Upper Atmospheric Research Sattelite (UARS)", *J. Geophys. Res.* 98, 10695-10711 (1993).

47. G.J. Rottman, et al., "Solar Stellar Irradiance Comparison Experiment 1 1: instrument design and operation", J. Geophys. Res. 98, 10667-10678 (1993).

48. R.P. Cebula et al., "Observations of the solar irradiance in the 200-350 nm interval during the ATLAS-1 mission: a comparison among three sets of measurements - SSBUV, SOLSPEC, and SUSIM", *Geoph. Res. Lett.*, 23, 289-2292 (1996).

49. T.N., Woods, et al., "Validation of the UARS solar ultraviolet irradiances: Comaparison with the ATLAS 1 and 2 measurements", *J.Geophys. Res.*, 101, 9541-9569 (1996).

50. S.C. Liu, S.A. McKeen, and S.Madronich, Effect of anthropogenic aerosols on biologically active ultraviolet radiation, *Geophys. Res. Lett.*, 18, 2265-2268 (1991).

51. R.R. Dickerson, S. Kondragunta, G.Stenchikov, K.L. Civerolo, B.G. Doddridge, and B.N. Holben, The impact of aerosols on Solar Ultraviolet radiation and Photochemical Smog, *Science*, 278, 827-830 (1997).

52. C. J. Erlick, J.E. Frederick, V.K. Saxena and B.N. Wenny, Atmospheric transmission in the ultraviolet and visible: aerosols in cloudy atmospheres, *J. Geophys. Res.*, 103, 31541-31556 (1998).

53. C.J. Erlick, and J.E. Frederick, Effects of aerosols on the wavelength dependence of atmospheric transmission in the ultraviolet and visible 2. Continental and urban aerosols in clear skies, *J. Geophys. Res.*, 103, 23275-23285 (1998).

54. Kylling, A., A.F. Bais, M. Blumthaler, J. Schreder, C.S. Zerefos, and E.Kosmidis, Effect of aerosols on solar UV irradiance during the photochemical activity and solar ultraviolet radiation campaign, *J. Geophys. Res.* 103, 26051-26060 (1998).

55. M.Z. Jacobson, Isolating nitrated and aromatic aerosols and nitrated aromatic gases as sources of ultraviolet light absorption, *J. Geophys. Res.* 104, 3527-3542 (1999).

56. W.J. Wiscombe and S.G. Warren, "A model for the spectral albedo of snow, I. Pure snow", J. Atmos. Sci. 37,2712-2733 (1980).

57. T.C. Grenfell, S. G. Warren, and P. C. Mullen, "Reflection of solar radiation by the Antarctic snow surface at ultraviolet, visible, and near-infrared wavelengths", *J. Geophys. Res.* 99, 18,669-18,684 (1994).

58. J. Lenoble, "Modeling of the influence of snow reflectance on ultraviolet irradiance for cloudless sky", *Appl.Opt.* 37, 2441-2447 (1998).

59. J.R. Herman and E. Celarier, "Earth surface reflectivity climatology at 340 to 380 nm from TOMS data," *J. Geophy. Res.*, 102, 28003-28011 (1997).

60. J.R. Herman, E. Celarier, and D. Larko, "UV 380nm reflectivity of the Earth's surface, clouds and aerosols," J. Geophys. Res. 106, 5335-5351 (2001).

61. W.B. Rossow and R.A.Schiffer, ISCCP cloud data products, *Bull. Am. Met. Soc.* 72, 2-20 (1991).

62. M.L. Nack, and A.E.S. Green, "Influence of clouds, haze and smog on the middle ultraviolet reaching the ground," *Appl. Opt.* 13, 2405-2415 (1974).

63. I.V. Geogdzhaev, T.V. Kondranin , A.N. Rublev, N.Ye.Chubarova , "UV Radiation Transfer Through Broken Cloud Fields Modeling and Comparison with Measurements", "Izvestiya, Atmospheric and Oceanic Physics", 33(5), 630-635 (1997).

64. J.T. Suttles, R.N.Green, G.L.Smith, B.A. Wielicki, I.J.Walker, V.R.Taylor, and L.L.Stowe, "Angular Radiation models for the Earth-atmosphere system. Vol. 1 Shortwave Radiation", NASA reference Publication RP-1184, 159 pp. (1989).

65. M. Blumthaler, and Ambach, W., "Solar UVB-albedo of various surfaces", *Photochem. Photobiol.* 48, 85-88 (1988).

66. B.L. Diffey, A.T.Green, M.J.Loftus, G.J.Johnston and P.S. Lee, "A portable instrument for measuring ground reflectance in the ultraviolet", *Photochem. Photobiol.* 61, 68-70 (1995).

67. A. Arola , J. Kaurola, T. Tikkanen, L. Koskinen, P. Taalas, J. Herman and N. Krotkov, "A new approach to estimate the albedo for snow-covered surface in space-borne UV retrieval method", submitted to *J. Geophys Res*, (2002).

68. J.R. Herman, JP.K.Bhartia, O.Torres, C.Hsu, C.Seftor, and E.Celarier, "Global distibution of UV-absorbing aerosols from Nimbus-7/TOMS data", *J.Geophys. Res.*, 102, 16911- (1997).

69. O. Torres, P.K. Bhartia, J.R. Herman, Z.Ahmad, "Derivation of aerosol properties from satellite measurements of backscattered ultraviolet radiation. Theoretical basis", *J Geophys Res*, 103, 17099-17110 (1998).

70. B.N. Holben, et al., "AERONET-A Federated Instrument Network and Data Archive for Aerosol Characterization", *Remote Sens. Environ.* 66, 1-16 (1998).

71. B.N. Holben, et al., "An emerging ground-based aerosol climatology: aerosol optical depth from AERONET", *J Geophys Res*, 106, 12067-12097 (2001).

72. A.Smirnov et al., "Optical properties of atmospheric aerosol in maritime environments", in print *J.Atmos. Sciences*, (2002).

73. O.Dubovik et al., "Variability of absorption and optical properties of key aerosol types observed in worldwide locations", in print *J.Atmos. Sciences*, (2002).

74. Eck et al., "Measurements of irradiance attenuation and estimation of aerosol single scattering albedo for biomass burning aerosols in Amazonia", *J Geophys Res*, 103, 31865-31878 (1998).

75. Eck et al., "Characterization of the optical properties of biomass burning aerosols in Zambia during the 1997 ZIBBEE field campaign", *J Geophys Res*, 106, 3425-3448 (2001).

76. R.L.McKenzie, G.Seckmeyer, , A.F.Bais, J.B.Kerr, and S. Madronich, "Satellite retrievals of erythemal UV dose compared with ground-based measurements at northern and southern midlatitudes", *J Geophys Res*, 106, 24051-24062 (2001).

Table 1 Expected errors in estimated surface flux at 310nm

Error source	SZA=0°	SZA=50°	sza=70°	sza=86°
Total Ozone (2% rms)	1.3%	2%	3%	< 3% (Umkehr)
Surface reflectivity snow/ice-free,1% rms (*snow/ice, 5% rms)	0.4% (3%)	0.4% (3%)	0.4% (3%)	0.5% (3%)
Strat profile (1/4 th of high-low difference)	0.5%	0.7%	0.3%	>30% (Umkehr effect)
Trop profile (5 DU rms)	0.5%	0.5%	0.2%	0.2%
Total rms	2% (3.6%)	2.8% (4%)	3.7%(4.7%)	>30%

The table concerns only cloud- and aerosol-free cases and gives lower limits of the uncertainties for horizontally homogeneous scenes over OMI footprint; (2) Numbers in parenthesis apply to snow/ice conditions for horizontally homogeneous surfaces with high surface albedo, $R_s > 0.7$ (Antarctic, Greenland). Over continents, a more realistic rms for snow/ice albedo would be at least 10-15%; (3) Errors do not include a ±3% uncertainty in absolute flux attributable to extra-terrestrial solar flux; (4)The uncertainty in long-term trend is 1%/decade (Herman et al. 1996), caused primarily by total ozone uncertainties; (5)The flux at 310nm has roughly the same ozone response as the erythema-weighted flux. Uncertainties in spectral flux at other wavelengths for $\theta_o < 50°$ can be approximately scaled relative to 310nm by using the following factors: 2 (at 305nm), 4 (at 300nm), and 6 (at 295nm). For $\theta_o > 50°$ the uncertainties in spectral flux can not be scaled because of the Umkehr effect.

Table 2 Expected Errors in UV-Irradiance Attenuation (AAC) algorithm due to uncertainty in estimated aerosol height, ΔH, for smoke and dust[31]. The error is proportional to both ΔH and aerosol absorption (single scattering co-albedo, 1-ω). The errors are shown in Table 2 for ΔH=0.5km. The largest error corresponds to the large-particle dust, which is also strongly absorbing[69].

Model/Parameter	ω	k	S (km^{-1})	E_F (%)
Smoke C1	0.92	0.25	12	1.5
Smoke C2	0.84	0.37	40	7.5
Dust D1	0.90	0.28	12	1.7
Dust D2	0.72	0.50	43	11
Dust D3	0.63	0.57	55	16

Figure captions

Figure 1. TOMS version 1 UV algorithm processes diagram

Figure 2. Comparison of original and improved cloudiness treatment in the UV algorithm. Liquid and ice water data of ECMWF (solid line) is used (assuming total overcast case) in the improved case. The improved method (Eq.4) shows better agreement with the Brewer daily observations (diamonds), whereas the original TOMS algorithm (Eq.3) gives an overestimate of the daily dose ~60% for this particular case.

Figure 3. Comparison of daily Erythemal (CIE) UV doses [J/m^2] calculated with original (Eq.3) and improved (Eq.4) cloudiness treatment in the TOMS UV algorithm with ground based Brewer observations at Sodankylä from 8 July to 1 September, 1992.

Figure 4. Fragment of he broken cloud field as model input. The model is based on the normal random (Gaussian) field with a fixed lower boundary [Geogdzhaev et al., 1997]. Spatially inhomogeneous cloud structure is described by 3D array of cells each with prescribed cloud properties. The dimensions of each cell should be sufficiently small compare to the photons free path. In most cases 50 to 100 meters cells were found to be sufficient in modeling TOMS and OMI FOVs. The dimensions of the calculated field are similar to a single OMI FOV (10km by 20km). Cloud cover 0.5, aspect ratio 1, scattering coefficient 50 km^{-1} and cloud average diameter 1km.

Figure 5. Anisotropic function $AIF(\theta_0, \theta, \varphi)$ of the broken cloud scene (figure 4) forθ_0=54° as a function of the satellite vertical angle, θ (giving by distance from the center of the figure – nadir direction) and solar azimuthal angle, φ (given by polar angle: forward reflecting in on the right and

backward reflecting – on the left). The AIF is defined as the ratio of the equivalent Lambertian flux to the actual reflected flux: $AIF = \pi L(\theta_0, \theta, \varphi) / M(\theta_0)$ [Suttles et al. 1988]. AIF <1 (shown by green color) means that the measured radiance is less than Lambertian and AIF>1 (red colors) means that the radiance for broken cloud scene is greater than Lambertian.radiance.

Figure 6. Example of a correction factor for broken cloud scene (figure 4), which should be applied to the satellite UV data calculated with TOMS method (i.e. using homogeneous plane-parallel cloud model). Depending on the satellite viewing direction (explained in figure 5) the correction factor ranges from 0.85 to 1.2. Cloud anisotropy is much less in the plane perpendicular to the solar principal plane than in the solar principal plane. Surface reflectivity 5%. Solar zenith angle 54°. The equivalent optical thickness of the homogeneous plane parallel cloud layer is close to 5.

Figure 7. The effect of the new snow albedo treatment on the computed surface UV. "TOMS original UV" is based on MLER [59,60] whereas "TOMS modified UV" is based on the snow albedo regression with ERA-15 snow depth data, and coincident and co-located Nimbus-7 TOMS reflectivity measurements[67]. Top: Comparison at Sodankylä, Finland; bottom: Churchill, Canada

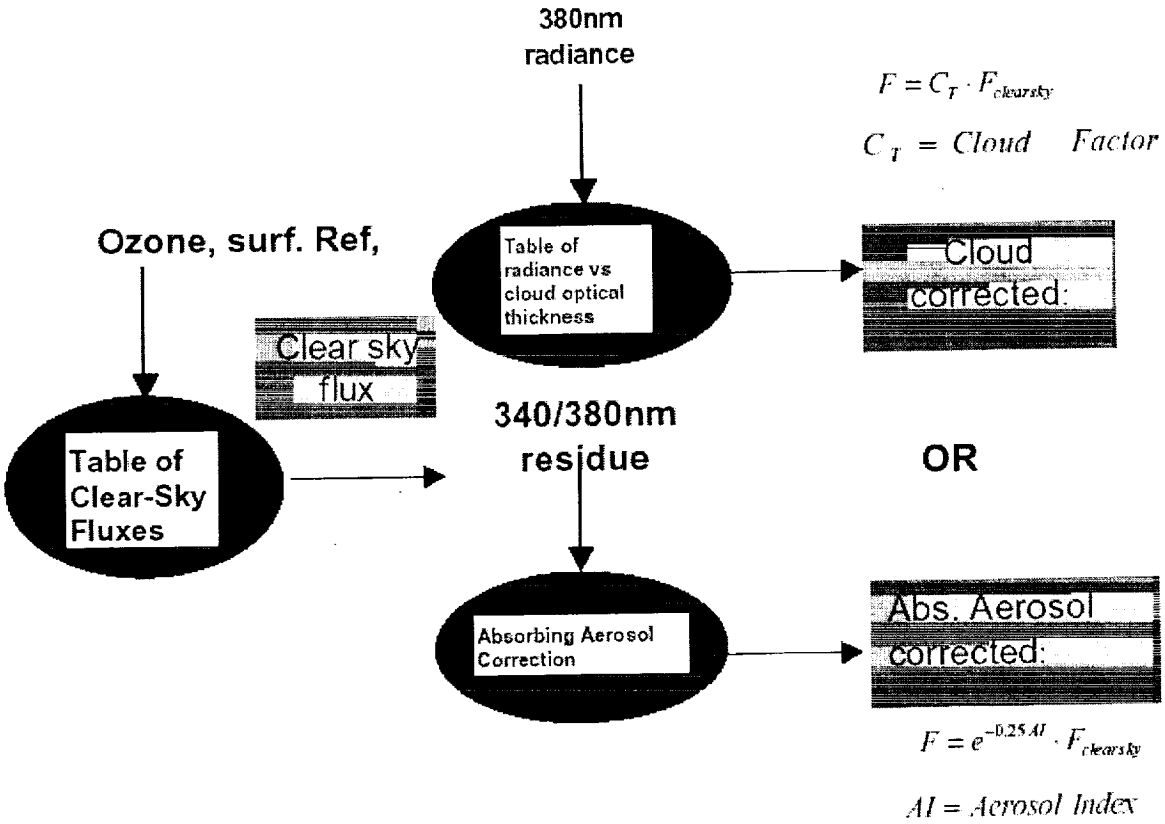

Figure 1 TOMS version 1 UV algorithm processes diagram

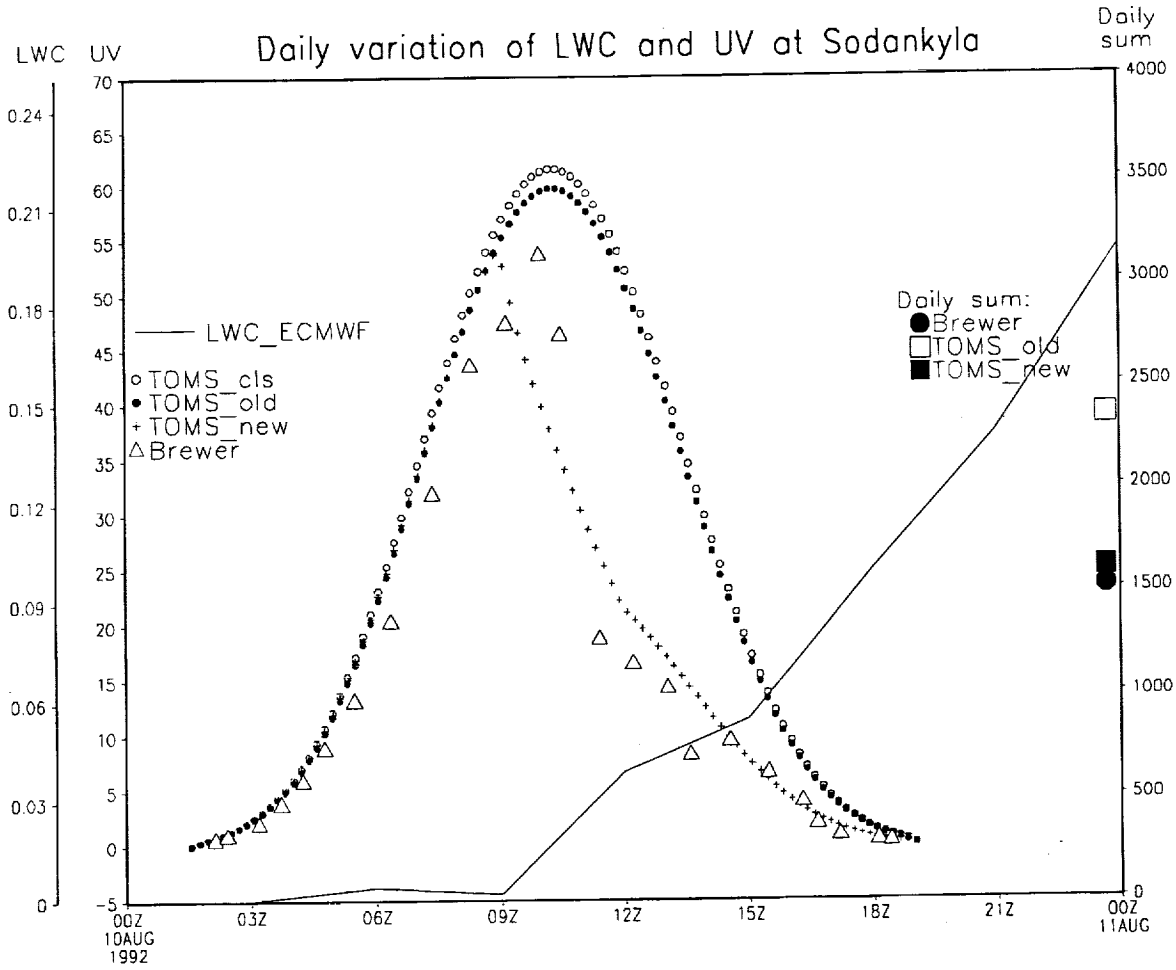

Figure 2. Comparison of original and improved cloudiness treatment in the UV algorithm. Liquid and ice water data of ECMWF (solid line) is used (assuming total overcast case) in the improved case. The improved method (Eq.4) shows better agreement with the Brewer daily observations (diamonds), whereas the original TOMS algorithm (Eq.3) gives an overestimate of the daily dose ~60% for this particular case.

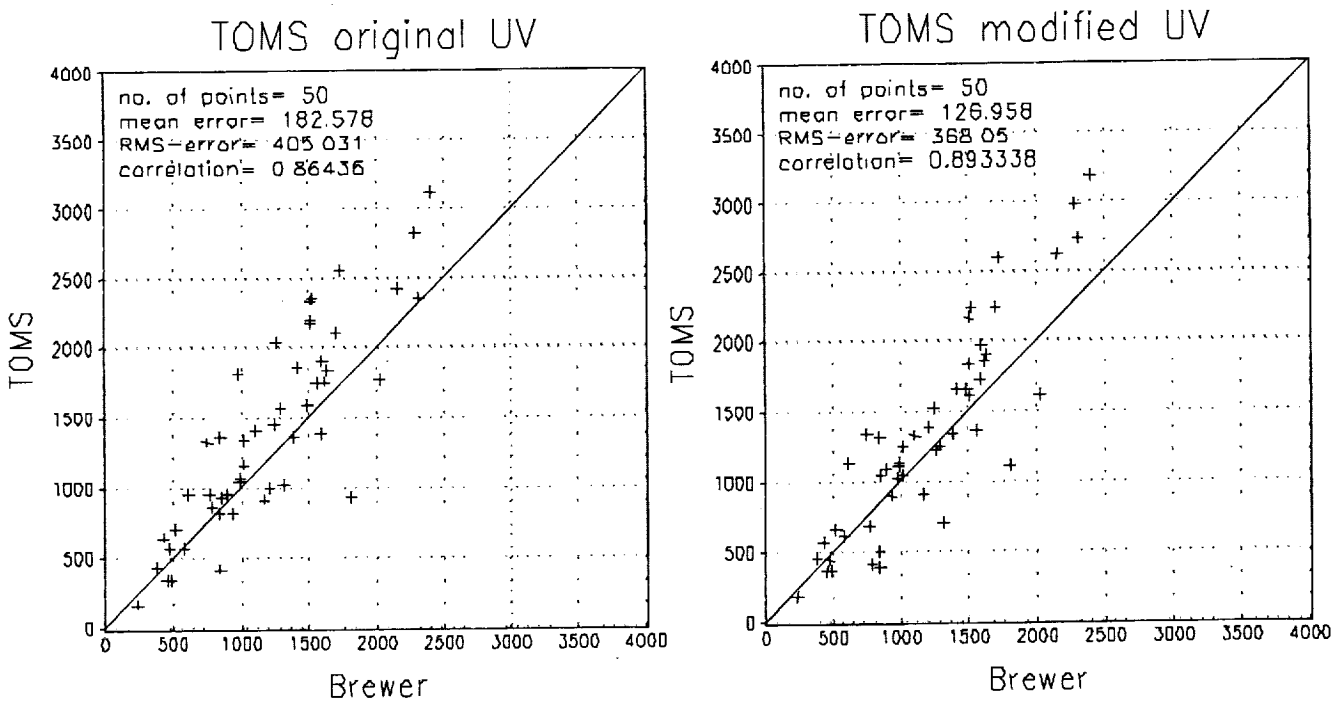

Figure 3. Comparison of daily Erythemal (CIE) UV doses [J/m^2] calculated with original (Eq.3) and improved (Eq.4) cloudiness treatment in the TOMS UV algorithm with ground based Brewer observations at Sodankylä from 8 July to 1 September, 1992.

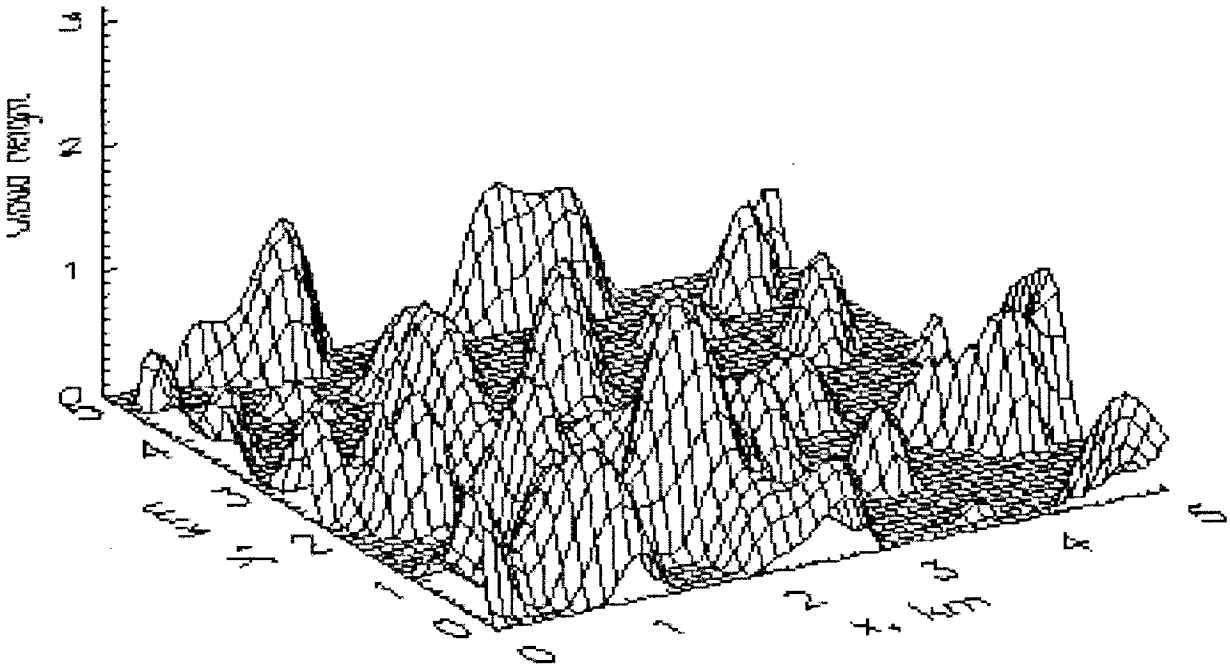

Figure 4

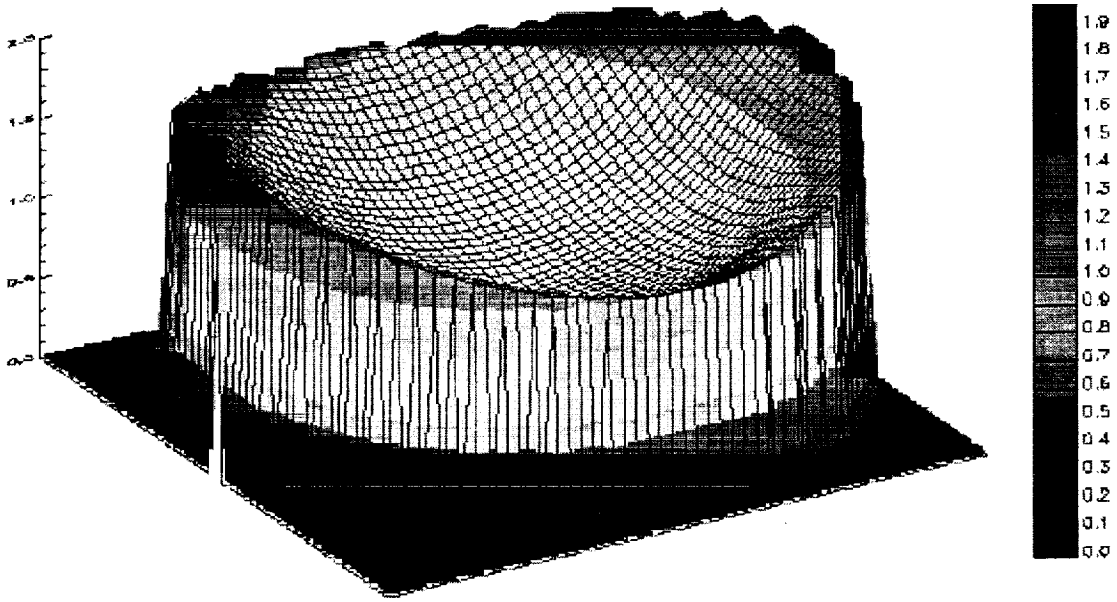

Figure 5. Anisotropic function $AIF(\theta_0, \theta, \varphi)$ of the broken cloud scene (figure 4) forθ_0=54° as a function of the satellite vertical angle, θ (giving by distance from the center of the figure – nadir direction) and solar azimuthal angle, φ (given by polar angle: forward reflecting in on the right and backward reflecting – on the left). The AIF is defined as the ratio of the equivalent Lambertian flux to the actual reflected flux: $AIF = \pi L(\theta_0, \theta, \varphi) / M(\theta_0)$ [Suttles et al. 1988]. AIF <1 (shown by green color) means that the measured radiance is less than Lambertian and AIF>1 (red colors) means that the radiance for broken cloud scene is greater than Lambertian.radiance.

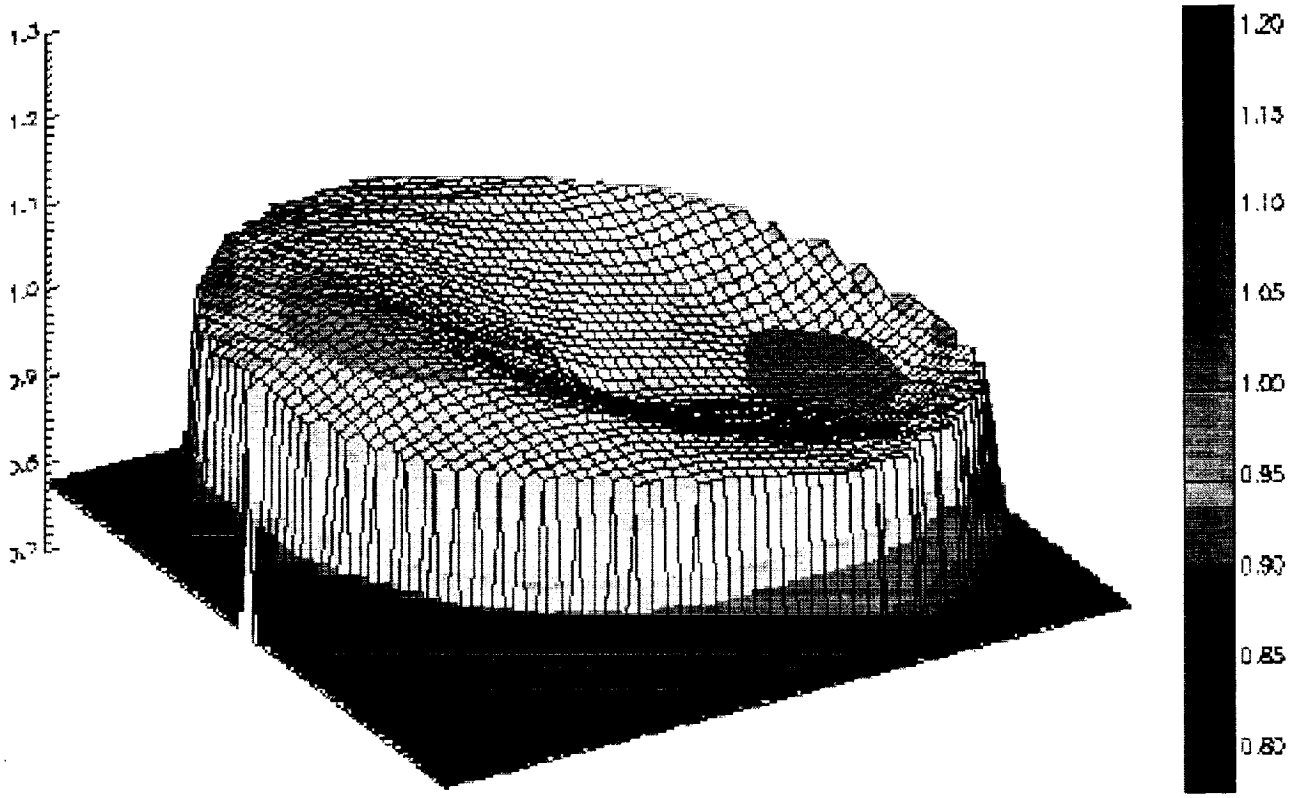

Figure 6. Example of a correction factor for broken cloud scene (figure 4), which should be applied to the satellite UV data calculated with TOMS method (i.e. using homogeneous plane-parallel cloud model). Depending on the satellite viewing direction (explained in figure 5) the correction factor ranges from 0.85 to 1.2. Cloud anisotropy is much less in the plane perpendicular to the solar principal plane than in the solar principal plane. Surface reflectivity 5%. Solar zenith angle 54°. The equivalent optical thickness of the homogeneous plane parallel cloud layer is close to 5.

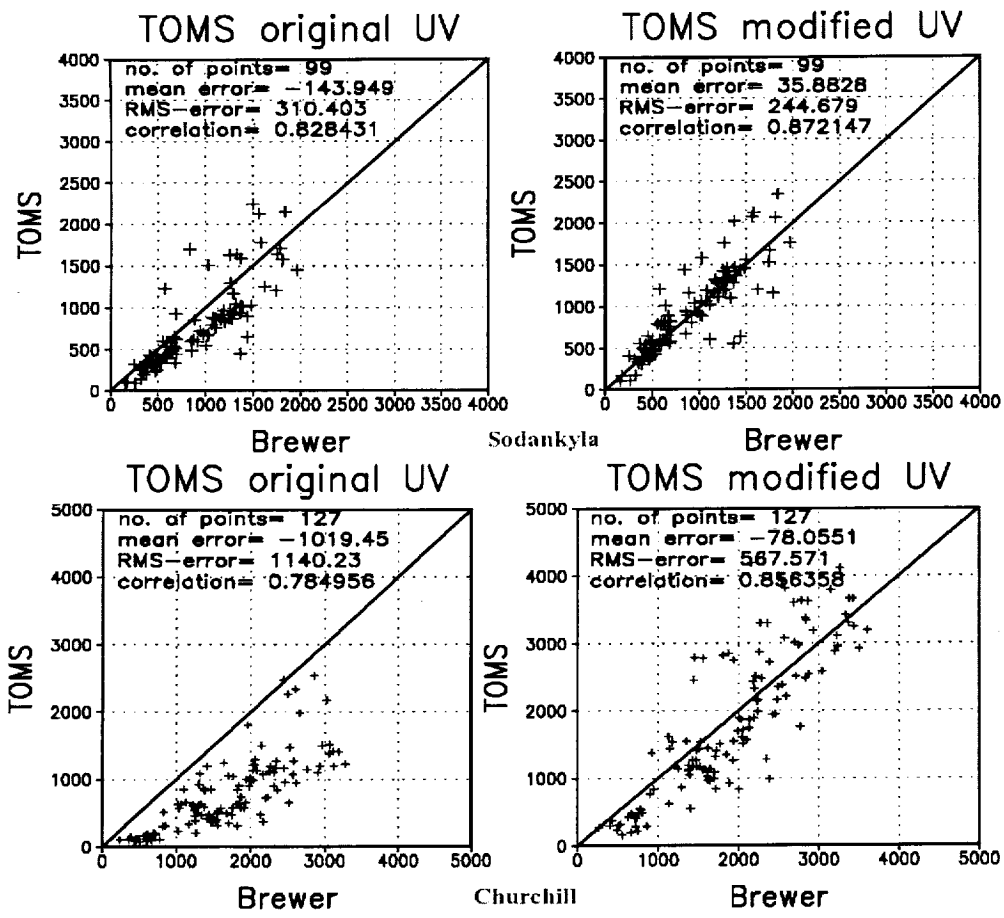

Figure 7. The effect of the new snow albedo treatment on the computed surface UV. "TOMS original UV" is based on MLER [59,60] whereas "TOMS modified UV" is based on the snow albedo regression with ERA-15 snow depth data, and coincident and co-located Nimbus-7 TOMS reflectivity measurements[67]. Top: Comparison at Sodankylä, Finland; bottom: Churchill, Canada

Popular Summary:

Version 2 TOMS UV algorithm: problems and enhancements

Nickolay Krotkov[1,2], Jay Herman[2], P.K.Bhartia[2], Colin Seftor[3], Antti Arola[4], Jussi Kaurola[4], Lasse Koskinen[4], S. Kalliskota [4], Petteri Taalas[4], I. Geogdzhaev[5]

Satellite instruments provide global maps of surface UV irradiance by combining backscattered radiance measurements with radiative transfer models. The models are limited by uncertainties in input parameters of the atmosphere and the surface. We evaluate the effects of possible enhancements of the current TOMS surface UV irradiance algorithm focusing on effects of diurnal variation of cloudiness and improved treatment of snow/ice. The emphasis is on comparison between the results of the current (version 1) TOMS UV algorithm and each of the changes proposed. We evaluate different approaches for improved treatment of pixel average cloud attenuation, with and without snow/ice on the ground. In addition to treating clouds based only on the measurements at the local time of the TOMS observations, the results from other satellites and weather assimilation models can be used to estimate attenuation of the incident UV irradiance throughout the day. A new method is proposed to obtain a more realistic treatment of snow covered terrain. The method is based on a statistical relation between UV reflectivity and snow depth. The new method reduced the bias between the TOMS UV estimations and ground-based UV measurements for snow periods. The improved (version 2) algorithm will be applied to re-process the existing TOMS UV data record (since 1978) and to the future satellite sensors (e.g., Quik/TOMS, GOME, OMI on EOS/Aura and Triana/EPIC).